On conditions at the sheath boundaries of a quasineutral code for Hall thrusters

IEPC-2005-041

Presented at the 29th International Electric Propulsion Conference, Princeton University, October 31 - November 4, 2005

D. Escobar* and E. Ahedo†

E.T.S.I. Aeronáuticos, Universidad Politécnica de Madrid, Madrid 28040, Spain

F.I. Parra‡

Massachusetts Institute of Technology, Cambridge, MA 02139, USA

Two-dimensional, quasineutral, hybrid codes for Hall thruster discharges require the solutions of space-charge sheaths at the anode and the ceramic walls in order to determine the conditions to be fulfilled at the simulation boundaries. Improved models for these sheaths, which take into account doubly-charged ions, supersonic Bohm conditions, and more correct electron populations are presented. Last advances on more accurate plasma weighting algorithms at the simulation boundaries are presented too.

I. Introduction

HPHall[1] was the first two-dimensional(2D), hybrid (particle/fluid) code developed for Hall thrusters. The code treats ions and neutrals with Particle-In-Cell(PIC) methods and electrons as a fluid. A key feature of HPHall is that it takes advantage of the small Debye length of the plasma to impose plasma quasineutrality. Thus, plasma density is computed from the PIC subcode and transmitted to the electron code, which mainly computes the electric potential and the electron temperature. This approach reduces drastically the computation time because it avoids the very short spatial and temporal scales associated with the space-charge sheaths formed around the chamber walls. The handicap is that the Debye sheaths must be solved independently and conditions at the boundaries of the computational domain correspond to sheath transition conditions and not to wall conditions.

Two recent papers[2,3] have demonstrated that the interaction with the sheaths affects strongly the profiles of the quasineutral plasma and the thruster performances. Thus, a reliable estimate of thruster efficiency and wall erosion needs of detailed sheath models that compute accurately particle fluxes and energy losses to walls.

HPHall-2,[4] an updated version of HPHall, used the model of Ahedo[5] for the lateral sheaths and the new weighting algorithms proposed in Refs.2, 3. This meant a clear advance over the first version but, at the same time, it was realized that further advances were needed. This paper presents the state of the research on this subject. The improvements discussed here are being implemented in a new simulation code presented in a parallel paper.[6] Section II is devoted to the sheath models at the anode and ceramic walls. Section III treats the magnitude weighting at the boundaries.

*Student, Departamento de Fundamentos Matemáticos, escobar@fmetsia.upm.es.

†Associate Professor, Departamento de Fundamentos Matemáticos, ahedo@fmetsia.upm.es.

‡M.S. Candidate, Department of Aeronautics & Astronautics, fparra@mit.edu.

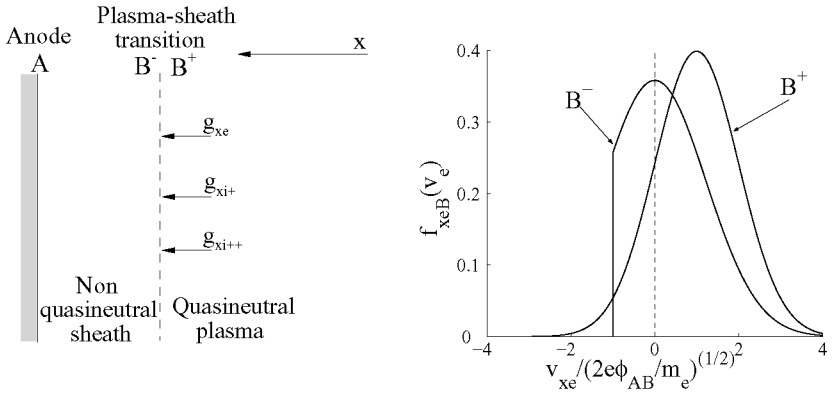

Figure 1. (a) Sketch of the anode sheath. (b) The truncated Maxwellian distribution at the sheath side of B, and the 'equivalent' drifted Maxwellian distribution corresponding to macroscopic magnitudes at the quasineutral side of B.

II. Improved sheath models

A. On the anode sheath model

A simple sketch of the anode is represented in figure 1(a). Because of its thinness, of the order of the Debye length, the sheath is considered collisionless, quasisteady, and, in principle, negative (meaning electron-repelling). Since the wall is considered metallic, the role of this sheath is to adjust the small, diffusive electron flux coming from the quasineutral plasma to the electron flux collected by the (perfectly-absorbing) anode. Hence, the main sheath characteristics depend only on electrons. The anode sheath model used by Fife, Ahedo et al.,[7,8] Dorf et al.,[9] and other researchers assumes a full Maxwellian distribution of electrons at the sheath entrance (point B). This model is inaccurate since the anode does not return back the electrons reaching it. Notice that a drifted Maxwellian, as assumed by Ahedo,[10] is incorrect too, since the distribution must be symmetric on the normal velocity for electrons that are reflected back within the sheath.

The correct choice, within the 'family' of Maxwellian distributions, is a truncated, zero-drift distribution. Thus, taking into account the energy conservation of the electrons within the sheath, one has

$$f_{xe}(v_{xe},\phi) = n_\star\sqrt{\frac{m_e}{2\pi T_\star}}\exp\Big(-\frac{m_e v_{xe}^2/2 + e(\phi_B-\phi)}{T_\star}\Big)H\Big(v_{xe}+\sqrt{\frac{2e(\phi-\phi_A)}{m_e}}\Big). \tag{1}$$

Here, f_{xe} is the one-dimensional(1D) function for the normal velocity component v_{xe}, the potential ϕ plays the role of the spatial variable $H(v_x)$ is the Heaviside step function of v_x, and $T_\star$ and $n_\star$ are constants characterizing the distribution. These constants are the temperature and density at B only in the limit of a non-truncated distribution.

Let us consider a one-dimensional problem where plasma magnitudes are constant along the whole surface transition B. If ϕ_{AB} is the sheath potential fall and taking the appropriate moments of f_{xe}, the density, particle flux, temperature, and total energy flux at B are

$$n_{eB} = n_\star\frac{1+\mathrm{erf}(\sqrt{e\phi_{AB}/T_\star})}{2}, \tag{2}$$

$$g_{xeB} = n_\star\sqrt{\frac{T_\star}{2\pi m_e}}\exp\Big(-\frac{e\phi_{AB}}{T_\star}\Big), \tag{3}$$

$$\frac{T_{eB}}{T_\star} = 1+\frac{m_e u_{xeB}^2}{3T_\star} - \frac{2}{3\sqrt{\pi}}\Big(\sqrt{\frac{2m_e u_{xeB}^2}{T_\star}}+\sqrt{\frac{e\phi_{AB}}{T_\star}}\Big)\frac{\exp\Big(-\frac{e\phi_{AB}}{T_\star}\Big)}{1+\mathrm{erf}(\sqrt{e\phi_{AB}/T_\star})}, \tag{4}$$

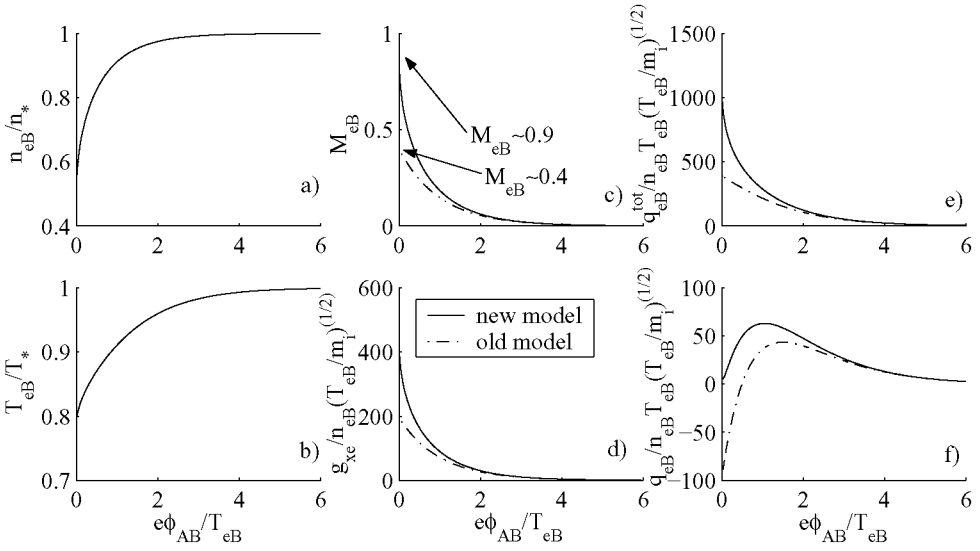

Figure 2. Comparison of anode models in terms of the non-dimensional electron density (a), non-dimensional electron temperature (b), electron Mach number (c), non-dimensional electron flux to anode (d), non-dimensional total energy flux to the anode (e) and non-dimensional heat flux to the anode (f).

$$q_{xeB}^{tot} = g_{xeB}(2T_\star + e\phi_{AB}), \tag{5}$$

respectively, with $u_{xe} = g_{xe}/n_e$ the macroscopic electron velocity and $\mathrm{erf}(x)$ the error function.

These magnitudes must match with those known from the quasineutral, macroscopic model for $x \geq x_B$. Therefore, these four equations determine the potential fall ϕ_{AB}, the constants of the distribution function, $n_\star$, $T_\star$, and the heat conduction flux to the wall, $q_{xeB} = q_{xeB}^{tot} - \frac{5}{2} g_{xeB} T_{eB}$.

Figure 2 compares the sheath parameters for the new and old (i.e. full Maxwellian) sheath models. As expected, both models coincide exactly for an infinite sheath potential fall and approximately for $e\phi_{AB}/T_{eB} > 3$. The old model[9,11] placed the transition to a no-sheath regime (i.e. ϕ_{AB}=0) at $M_{eB} = (2\pi)^{-1/2} \simeq 0.4$, with $M_{eB} \equiv |u_{xeB}|/\sqrt{T_{eB}/m_e}$ the electron Mach number. The present model places it at $M_{eB} \sim 0.9$, much closer to $M_{eB} = 1$ where the quasineutral, macroscopic model of Ahedo[10] places the transition from a negative- to a positive- anode sheath (for near-cold ions). [A perfect parametric matching of the quasineutral and kinetic models is unlikely since they have been postulated independently.] Notice that the increment of g_{xe}/n_{eB} and q_{xeB}^{tot}/n_{eB} as the sheath vanishes is due to the increase of u_{xeB} and decrease of n_{eB}, and not to changes of g_{xe}. Finally, another merit of the new model is that heat conduction to the anode is positive always; the old model predicted a negative heat conduction to the anode in the no-sheath limit, which did not look satisfactory.

In the preceding analysis ions have played no role. The Bohm condition states that the ion flux must enter sonic-supersonically into a *negative* sheath. The fulfillment of this condition pertains to the PIC subcode and, particularly, to the subject of plasma weighting at the domain boundaries.

B. On the sheath model at ceramic walls

The sheath around ceramic walls is more complex, since (i) both the electron and ion dynamics must be taken into account, (ii) there is secondary electron emission (SEE) by electron impact in the walls, and (iii) space-charge saturation is possible.[12]

Improvements on the sheath model are being implemented on three points. First, the use of truncated Maxwellian distribution for electrons, instead of the full Maxwellian distribution used originally by Hobbs and Wesson[12] and adopted by Ahedo.[5] Second, the inclusion of doubly-charged ions as an additional species, since they constitute a non-marginal population for high specific impulse operation.[6,13] And third, the consideration of a supersonic ion flux as a likely sheath entrance condition, because of the discharge

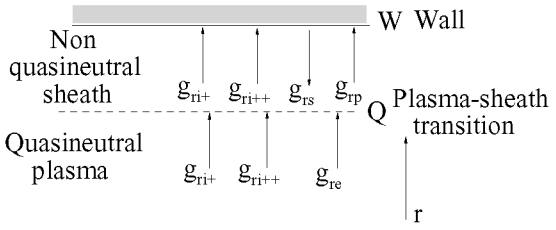

Figure 3. Sketch of ceramic wall fluxes and nomenclature.

fluctuations. With respect to this last point, we know that the Bohm condition for the sheath states that ions must enter sonically or supersonically. At the same time, the stationary (and macroscopic) solution for the quasineutral plasma states that ions must enter into the sheath subsonically or sonically. However, supersonic ion fluxes are possible in a time-fluctuating quasineutral solution, as Parra et al.[2] showed. Finally observe that the sheath remains quasi-steady for a fluctuating discharge (except for extremely large frequencies).

The fundamentals of the improved model are those set by Ahedo[5] except, of course, for the aspects we want to improve. We omit here the derivation of the model and just include some notes on it. A sketch of the ceramic wall sheath is shown in figure 3. The plasma species within the sheath are: primary electrons(p) coming from the quasineutral plasma, secondary electrons(s) emitted by the wall, singly-charged ions($i+$) and doubly-charged ions($i++$). Primary and secondary electrons match into a single electron population (e) outside the sheath. Quasi cold beams are assumed for the non-confined populations ($i+$, $i++$, and s). The zero current condition leads to

$$g_{ri+W} + 2g_{ri++W} = (1 - \delta_w) g_{rpW}, \tag{6}$$

where g_r mean particle flux perpendicular to the (radial) wall, and δ_w is the effective SEE yield.

Plasma quasineutrality at the sheath entrance yields

$$n_{sQ} + n_{pQ} \equiv n_{eQ} = n_{i+Q} + 2n_{i++Q} \tag{7}$$

and the average ion charge number for ions at point Q is

$$Z_{iQ} = \frac{n_{eQ}}{n_{iQ}} = \frac{n_{i+Q} + 2n_{i++Q}}{n_{i+Q} + n_{i++Q}}. \tag{8}$$

When there is only one ion beam, the Bohm condition of the sheath is explicit for the ion macroscopic velocity, Eq.(18) of Ref.5. In the presence of singly-charged and doubly-charged ion beams the Bohm condition yields

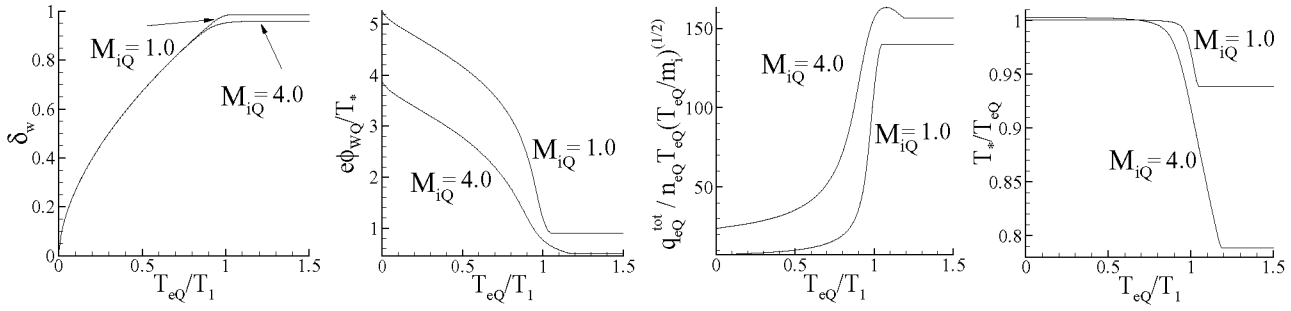

Figure 4. Ceramic material sheath model non-dimensional results and influence of the supersonic ion flow on the sheath properties.

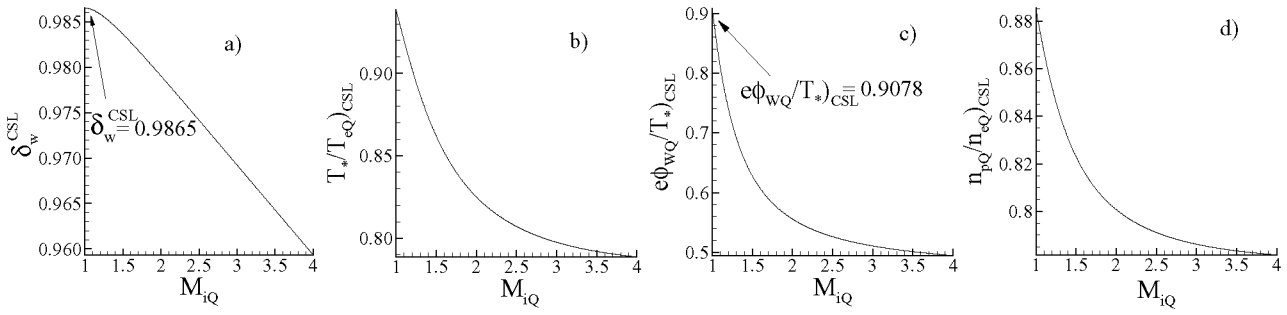

Figure 5. Influence of the ion Mach number on the properties at the saturation charge limit. SEE yield at CSL(a), non-dimensional temperature(b), non-dimensional sheath potential fall(c) and non-dimensional primary-electron density (d).

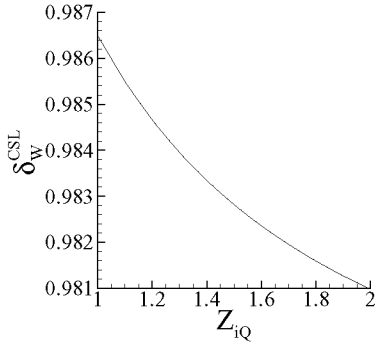

Figure 6. Influence of the equivalent charge number on the charge saturation limit.

only one relation between the two beam velocities. A correct closure of the problem would require to involve the presheath solution, and this would very costly. Two simple, alternative procedures are being studied. First, to take

$$u_{ri++Q} = \sqrt{2}u_{ri+Q} \tag{9}$$

as if the two ion beams were accelerated freely in the presheath, with no ion production. Second, to consider a single ion beam of charge Z_{iQ}. Results here are presented for the first alternative.

The sheath potential fall, ϕ_{WQ}, turns out to verify

$$\frac{e\phi_{WQ}}{T_\star} = \ln\sqrt{\frac{m_i}{2\pi m_e}} + \ln(1-\delta_w) + \ln\left(\frac{n_{pQ}}{n_{eQ}}\sqrt{\frac{T_\star}{T_{eQ}}}\right) - \ln\left(2\sqrt{2}-1-2(\sqrt{2}-1)/Z_{iQ}\right) - \ln M_{iQ} - \ln\frac{1+\mathrm{erf}\left(\sqrt{e\phi_{WQ}/T_\star}\right)}{2}, \tag{10}$$

where the second line groups the effects newly introduced: doubly-charge ions, $Z_{iQ} > 1$, supersonic ion flux $M_{iQ} = u_{i+Q}/\sqrt{T_{eQ}/m_i}$, and truncated Maxwellian distribution (based on 'temperature' $T_\star$) for primary electrons (yielding the term with the error function).

This new model depends on three dimensionless parameters coming from the quasineutral solution (i.e. from the simulation of the 2D discharge) and the wall material: T_{eQ}/T_1 (with T_1 the temperature for a 100% SEE yield[5]) M_{iQ}, and Z_{iQ}. Figure (4) shows that the ion Mach number is found to affect significantly the potential fall and, thus the energies of ions and electrons impacting the wall. The influence of the ion charge number can be interpreted as an increase of ion Mach number, as Eq. (10) shows. Since, according to Ref.6, Z_{iQ} is between 1 and 1.1 its effect is small.

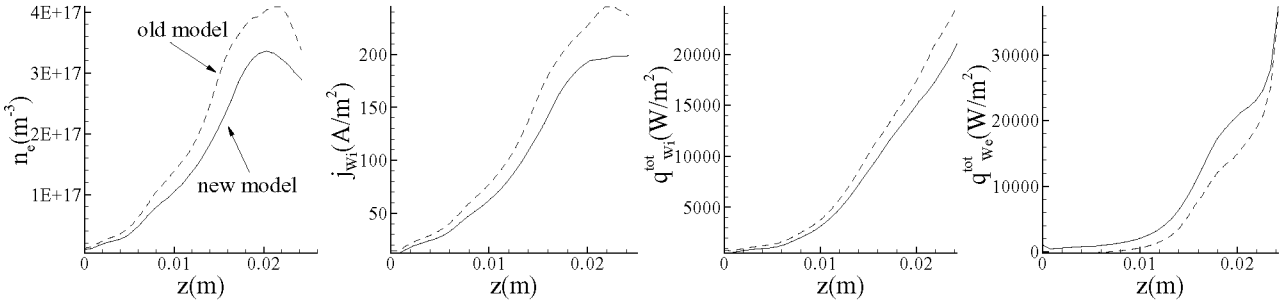

Figure 7. Plasma characteristics at the outer wall with the new (solid lines) and old (dashed lines) models for the lateral sheaths. The simulation data is the same used in Ref.6.

In the present model the charge saturation limit(CSL) is not universal, but depends on two parameters, M_{iQ} and Z_{iQ}. This is illustrated in figures (5) and (6). Both new effects tend to reduce the value of the SEE yield at the CSL, thus reducing the electron energy losses to the walls.

Finally, the use of a truncated distribution function for primary electrons at Q introduces modifications only at the CSL or close to it. For the basic case, $M_{iQ} = 1$ and $Z_{iQ} = 1$, Hobbs and Wesson had δ_W^{CSL} =0.983, whereas now we find δ_W^{CSL} =0.9865. One can be tempted to neglect this 0.3% difference on δ_W^{CSL}, unless one realizes that the important magnitude is $1/(1-\delta_w^{CSL})$ which measures particle and energy fluxes to the walls. Then, one finds that the differences in energy deposition with Hobbs-Wesson amount to a 25% (larger in the present case).

Figure 7 displays a comparison of the results obtained with the simulation code of Ref.6 using the old and new models for the lateral sheaths.

III. Weighting at the domain boundaries

References 2 and 3 showed that a correct weighting of plasma magnitudes at the boundaries of the quasineutral computational domain was a delicate issue. In this section we review the methods that have been used in HPHall and HPHall-2 and we present a new scheme which compares advantageously with previous ones. The influence of the different schemes over the temporal oscillations is briefly discussed too.

Figure 8 shows the geometry, the two test meshes and the magnetic field profile used in this section work. Parameters correspond to a SPT-70 thruster. To facilitate the understanding of wall effects, we use a rather simple geometry and a B-field satisfying $B_z = 0$ and $B_r \propto 1/r$; in this way $\nabla \cdot \boldsymbol{B} = 0$, but $\nabla \times \boldsymbol{B} \neq \boldsymbol{0}$.

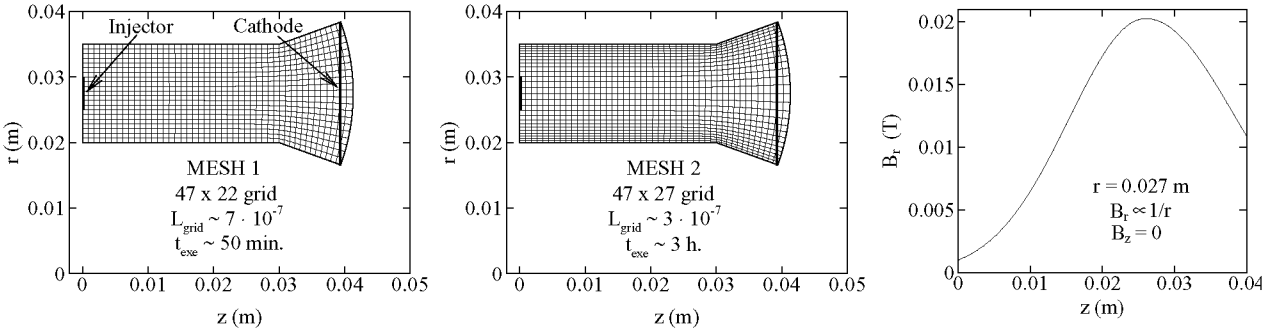

Figure 8. Geometry, test meshes and B-field for this work. Typical execution times (for a Pentium III at 2.4 GHz) to reach a steady-state response are included.

A. Weighting schemes

1. *Volumetric Weighting(VW)*

This is the original scheme used by Fife.[1] With this scheme, the magnitudes at nodes placed along the domain boundaries are computed using the typical PIC weighting algorithm. The ion density at a generic node T is determined from

$$(n_{eT})_{\mathrm{VW}} = \frac{1}{\Delta V_T} \sum_p \frac{Z_p m_p}{m_i} S_T(r_p, z_p), \tag{11}$$

where ΔV_T is the volume associated to node T, p refers to a particle being within the volume of influence of the node, m_p and (z_p, r_p) are particle mass and position, Z_p is one for single ions and two for double ions, and $S_T(r_p, z_p)$ is a bi-linear type weighting function for node T. This algorithm was applied to boundary nodes, even though the volume of influence at the boundaries is different (see Figure 6 of Ref. 3). The one-side, asymmetric weighting at the boundary nodes tends to underestimate [overestimate] magnitudes that increase [decrease] toward the boundary. The error can be large for magnitudes that present large gradients near the sheath boundary (which include n_e, $\boldsymbol{v}_i$, and ϕ, but not $\boldsymbol{j}_i$).

In 2 we demonstrated that, using VW and as the cell size of the mesh is reduced, the ion flow at the boundary increases significantly and larger plasma gradients over the whole radial section develop. However, for the mesh sizes the ion flow remains well subsonic (i.e. still far from satisfying the Bohm condition), making it evident that a different numerical approach should be used in order to weight correctly magnitudes at the boundaries.

2. *Corrected Volumetric Weighting(CW)*

This scheme was proposed in Ref.3. The idea is to use the information of two nodes [the one in the boundary(T) and the internal one next to it(T+1)] in order to correct the $O(\Delta r)$ error induced by the asymmetric VW. With the information of two nodes, the error can be reduced to $O(\Delta r^2)$. The corrected plasma density is,

$$(n_{eT})_{\mathrm{CW}} = \frac{3}{2}(n_{eT})_{\mathrm{VW}} - \frac{1}{2}(n_{e,T+1})_{\mathrm{VW}}, \tag{12}$$

with $(n_e)_{\mathrm{VW}}$ the plasma density obtained from the VW. $(n_{eT})_{\mathrm{CW}}$ is smaller than $(n_{eT})_{\mathrm{VW}}$ for usual conditions. This correction lies on internal (i.e. PIC-computed) magnitudes only, but, at the same time, it depends on a second node, and thus errors depend on the cell size. Reference 3 proved the CW algorithm to give a reasonable fulfillment of the Bohm condition if the mesh is fine enough.

3. *Surface Weighting (SW)*

Although the CW algorithm was promising, the need of a fine mesh was evident. The idea of SW is to count the particles that cross the surface of influence of the node at the boundary. Thus, SW is a PIC-intrinsic algorithm but, at the same time, is independent of the cell size.

The density n_e in the boundary node T,a s computed by SW, is

$$(n_{eT})_{\mathrm{SW}} = \frac{1}{\Delta S_T \Delta t} \sum_p \frac{Z_p m_p}{m_i} \frac{1}{\boldsymbol{v}_p \cdot \hat{\boldsymbol{N}}}, \tag{13}$$

where the sum extends to all the ions that have crossed the boundary, $\hat{\boldsymbol{N}}$ is the normal to the wall, ΔS_T is the surface of influence of node T, and Δt is the timestep used by the PIC code.

This computation for n_{eT} can be used whenever the flow of particles is only in one direction, like in the boundary, where no ions are coming back. The obtained $(n_{eT})_{\mathrm{SW}}$ is a time average in Δt of n_{eT}, and its error is only $O(\Delta r^2)$ (associated to the discretization of the electric potential, mainly).

Similarly, the ion current density at the boundaries is given by

$$(\boldsymbol{j}_{iT})_{\mathrm{SW}} = \frac{e}{\Delta S_T \Delta t} \sum_p \frac{Z_p m_p}{m_i} \frac{\boldsymbol{v}_p}{\boldsymbol{v}_p \cdot \hat{\boldsymbol{N}}}. \tag{14}$$

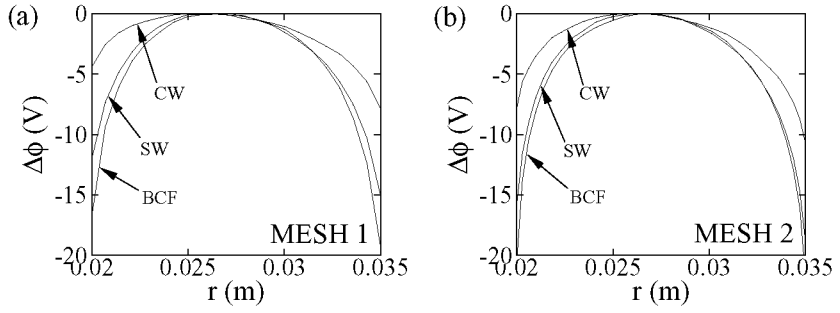

Figure 9. Radial profiles of electrostatic potential in $z = 0.0256$ m. (a) Comparison of results with the different algorithms in mesh 1. (b) Comparison of results with the different algorithms in mesh 2.

4. Bohm Condition Forcing (BCF)

This algorithm was presented in Ref.3. It consisted on forcing the ion flux to satisfy the (simple form of the) Bohm condition

$$\boldsymbol{j}_i \cdot \hat{\boldsymbol{N}} \geq n_e \sqrt{ZT_e/m_i} \tag{15}$$

whenever this was not achieved naturally by the VW algorithm; Z is the average ion charge-number. This the BCF algorithm for the density is

$$(n_{eT})_{BCF} = \min \left\{ \frac{(\boldsymbol{j}_{iT})_{\mathrm{SW}} \cdot \hat{\boldsymbol{N}}}{e\sqrt{ZT_e/m_i}}, (n_{eT})_{\mathrm{VW}} \right\} \tag{16}$$

With this algorithm, n_{eT} is lower in most points and instants than in the VW and, therefore, the electric field is larger near the boundaries. In Ref. 3 we showed that this algorithm provides excellent results even for relatively coarse meshes. This algorithm, contrary to the previous ones, relies on a property dictated by the space-charge sheath and, hence, extrinsic to the PIC code.

B. Comparison of profiles for the different schemes

Figure 9 shows some radial profiles obtained with different algorithms and mesh sizes. The new SW is, like CW, intrinsic to the PIC model, but at the same time provides reasonably good results even for coarse meshes. The presheath potential drop for SW and mesh 1 is around 75% of the potential drop achieved with BCF, and the difference decreases to 5% just by dividing by two the mesh size around the walls. This large difference is mainly due to the steep slope that exists in the density and potential profiles near the

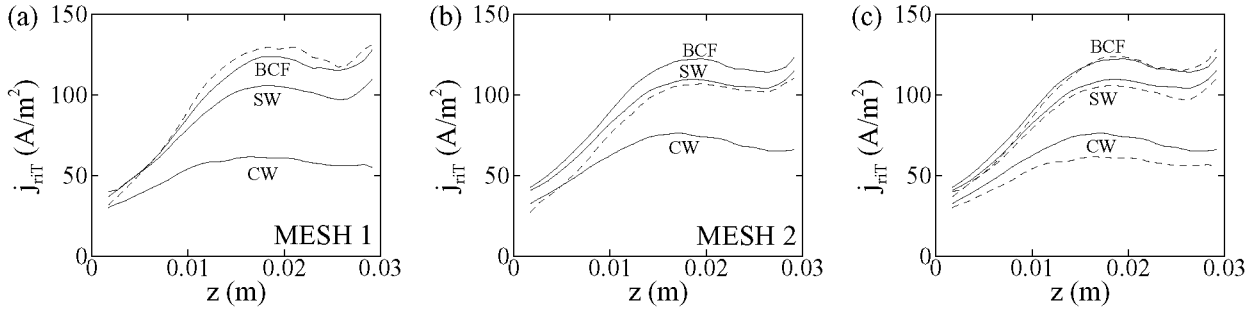

Figure 10. Axial profiles of ion current density to the inner wall for (a) mesh 1 and (b) mesh 2. In figures (a) and (b), the dashed line is the theoretical Bohm flux (j_{Bohm}) for SW and the corresponding mesh. (c) Comparison of sensitivities to the mesh size of CW, SW and BCF. Dashed lines represent results for mesh 1 and solid lines represent results for mesh 2.

boundaries of the quasineutral domain. Other magnitudes, like the ion density current flow to the walls ($\boldsymbol{j}_{iT}$) does not change as dramatically (see figure 10). The radial potential drop is not adequate to estimate the numerical errors induced by the hybrid model because it is very sensitive to the values near the boundaries, where the slope is extremely high. Magnitudes with flatter slopes are probably more suitable to analyze the accuracy of the schemes (as it is the case of $\boldsymbol{j}_{iT}$). However, radial profiles and their development give a good understanding of the problem, even if the exact values at the boundary are too sensitive to take them into account. Using $\boldsymbol{j}_{iT}$ as a criterium, we probably can say that BCF and SW are more accurate, since the change in ion flow with the mesh size is not as high as it is in CW.

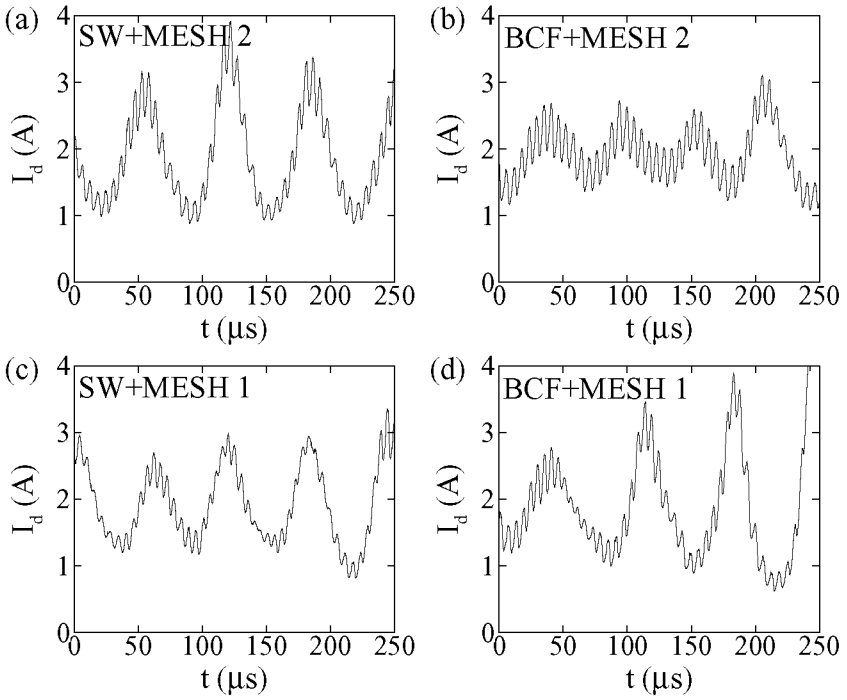

Figure 11. Time evolution of discharge current for different schemes and mesh sizes.

As observed in Ref. 2, the ion flow to the walls increases when the cell size decreases. Also, the schemes that provide more accuracy (BCF and SW) give a bigger ion flow to the walls. The ion flow can even be double with BCF and SW than it is with CW. Although BCF and SW have similar accuracy - if we consider the sensitivity to mesh size a measure of the error -, there is a difference in the ion flow at the exit of the channel. This difference is small compared to the difference between those schemes and CW or VW, but it is still important and remains to be studied.

In figures 10(a) and 10(b) the resulting ion flow with SW is compared to the simple Bohm condition (16). With mesh 1, both results differ greatly, probably due to the very different values of n_e at the boundaries (we have already commented the sensitivity of boundary values). The comparison is much better for mesh 2, where both values are practically the same.

To sum up, surface Weighting and Bohm Condition Forcing yield the best results. The Corrected Weighting requires too fine of a mesh, although it can be good to confirm the results given by the two other methods. Between SW and BCF, SW has the advantage of being more self-consistent since it is PIC-intrinsic. If the error is estimated from the sensitivity of the current to the wall with respect to the mesh size, BCF and SW have similar performance. SW fits the Bohm condition (16) for reasonable mesh sizes, which confirms its accuracy.

C. Discharge oscillations

One of the uses of simulation codes is the study of plasma oscillations in Hall thrusters. Therefore, the effect of the different schemes on time oscillations is an important criterium to decide how appropriate the

different schemes are. In figure 11, we present some time profiles for the discharge current. Two well-defined frequencies appear: one around 15 kHz, which seems to be related to the breathing mode, and another one near 170 kHz, which is, approximately, the ion transit frequency. These frequencies do not change with the mesh size or the weighting scheme, but their amplitude depends greatly on these parameters. The 15-kHz-oscillation amplitude is highly dependent on the weighting scheme: for mesh 2, the amplitude jumps from 35% for SW to 15% for BCF. It happens similarly for mesh 1. In the case of BCF, there must be two modes very near 15 kHz that produce, when they are added, the variable amplitude seen in figures 11(b) and 11(d) (it is especially clear in this last one). On the other hand, the 170 kHz oscillation is not as dependent on the weighting scheme. For mesh 2, its amplitude is 15% of the average current with both BCF and SW. For mesh 1, the amplitude decreases to 8% when we are using SW and is, again, around 15% with BCF. BCF seems to be able to reproduce this mode correctly for coarse meshes, whereas with SW the amplitude of the high frequency oscillations is rather dependent on mesh size.

To sum up, BCF perturbs less the 170 kHz mode, but it provokes a variable amplitude for the breathing mode, perhaps due to the superposition of two modes of very similar frequency. SW is not as effective reproducing the high frequency oscillations as BCF is, but with fine enough mesh SW yields the same amplitude. There are still important differences in the breathing mode between both schemes, which remain to be studied.

Acknowledgments

This work was sponsored by the Ministerio de Educación y Ciencia(MEC) of Spain (Project ESP2004-03093). D.E. was financed by a scholarship of the MEC.

References

[1]Fife, J. M., *Hybrid-PIC Modeling and Electrostatic Probe Survey of Hall Thrusters*, Ph.D. thesis, Massachusetts Institute of Technology, 1998.

[2]Parra, F., Ahedo, E., Martínez-Sánchez, M., and Fife, J., "Improvement of the plasma-wall model on a fluid-PIC code of a Hall thruster," *SP-555: 4th Spacecraft Propulsion Conference, Sardinia (Italy)*, European Space Agency, Noordwijk, The Netherlands, 2004.

[3]Parra, F. and Ahedo, E., "Fulfillment of the Bohm condition on the HPHall fluid-PIC code," *Proc. 40th Joint Propulsion Conference, Fort Lauderdale, FL*, AIAA 2004-3955, American Institute of Aeronautics and Astronautics,Washington, DC, 2004.

[4]Parra, F., Ahedo, E., Martínez-Sánchez, M., and Fife, M., "A two-dimensional hybrid model of the Hall thruster discharge," (to be submitted).

[5]Ahedo, E., "Presheath/sheath model of a plasma with secondary emission from two parallel walls," *Physics of Plasmas*, Vol. 9, No. 10, 2002, pp. 4340–4347.

[6]Escobar, D., Antón, A., and Ahedo, E., "Simulation of high-specific-impulse and double-stage Hall thrusters," *Proc. 29th International Electric Propulsion Conference, Princeton, USA*, IEPC-2005-040, Electric Rocket Propulsion Society, Cleveland, OH, 2005.

[7]Ahedo, E. and Martínez-Sánchez, M., "One-dimensional plasma structure in Hall thruster," *Proc. 34th Joint Propulsion Conference, Cleveland, OH*, AIAA-98-8788, American Institute of Aeronautics and Astronautics,Washington, DC, 1998.

[8]Ahedo, E., Gallardo, J., and Martínez-Sánchez, M., "Model of the plasma discharge in a Hall thruster with heat conduction," *Physics of Plasmas*, Vol. 9, No. 9, 2002, pp. 4061–4070.

[9]Dorf, L., Semenov, V., and Raitses, Y., " Anode sheath in Hall thrusters ," *Applied Physics Letters*, Vol. 83, No. 13, 2003, pp. 2551 – 2553.

[10]Ahedo, E., "On the near anode region of the Hall thruster discharge," *Proc. 40th Joint Propulsion Conference, Fort Lauderdale, FL*, AIAA 2004-3774, American Institute of Aeronautics and Astronautics,Washington, DC, 2004.

[11]Ahedo, E. and J.Rus, "Vanishing of the negative anode sheath in a Hall thruster," *Journal of Applied Physics*, Vol. 98, 2005, pp. 043306.

[12]Hobbs, G. and Wesson, J., " Heat flow through a Langmuir sheath in the presence of electron emission ," *Plasma Physics*, Vol. 9, 1967, pp. 85–87.

[13]Hofer, R. R. and Gallimore, A. D., "Efficiency Analysis of a High-Specific Impulse Hall Thruster," *40th Joint Propulsion Conference, Fort Lauderdale, FL*, AIAA-2004-3602, American Institute of Aeronautics and Astronautics,Washington, DC, 2004.